Nuclear Instruments and Methods in Physics Research 73 (1993) 403–412
North-Holland

NIM B
Beam Interactions with Materials & Atoms

Accelerator mass spectrometry of ^{59}Ni in extraterrestrial matter

W. Kutschera, I. Ahmad, B.G. Glagola, R.C. Pardo and K.E. Rehm
Physics Division, Argonne National Laboratory, Argonne, IL 60439, USA

D. Berkovits and M. Paul
Racah Institute of Physics, Hebrew University, Jerusalem 91904, Israel

J.R. Arnold and K. Nishiizumi
Dept. of Chemistry, University of California, San Diego, La Jolla, CA 92093, USA

Received 14 August 1992 and in revised form 15 October 1992

Cosmic-ray produced ^{59}Ni ($t_{1/2}$ = 76000 years) was detected in meteoritic and lunar material by AMS with fully stripped ions. At 641 MeV beam energy, a clean separation of $^{59}Ni^{28+}$ ions from $^{59}Co^{27+}$ background was achieved with a magnetic spectrograph. A background limit of $^{59}Ni/Ni < 7\times10^{-14}$ was determined with a blank Ni sample. A $^{59}Ni/Ni$ ratio of $(2.3\pm0.4)\times10^{-11}$ was measured in a sample from the Admire stony-iron (pallasite) meteorite, corresponding to a specific activity of 280 ± 50 dpm/kg meteorite. In a surface layer of Apollo 16 lunar rock 68815, a $^{59}Ni/Ni$ ratio of $(8.8\pm3.3)\times10^{-13}$ was measured (diluted with Ni carrier), corresponding to a specific activity of 4.1 ± 1.5 dpm/kg rock. This result compares well with values calculated by Reedy from the $^{56}Fe(\alpha, n)^{59}Ni$ reaction induced by solar cosmic ray alpha particles. Methodological aspects of the full-stripping technique and future possibilities of ^{59}Ni measurements in lunar materials are discussed.

1. Introduction

Long-lived radionuclides store information on the history of cosmic rays through their production in a variety of solar system materials [1]. Earth, moon and meteorites are the natural targets man has access to. From these three targets, only the lunar surface is capable of storing information of radionuclides produced by the relatively low energy of solar cosmic ray (SCR) particles. SCR particles are stopped within 3 g/cm^2 or less. In essence, only the top few millimeters of lunar surface contain the information on SCR particles. Deeper layers of lunar material, as well as meteorites, are the storehouses for radionuclides produced by the more energetic galactic cosmic ray (GCR) particles. On earth, the thick atmosphere (1000 g/cm^2) prevents the observation of SCR particles. Meteorites, on the other hand, lose surface layers containing SCR-produced nuclides during their fiery entrance to earth. The rich harvest of Apollo space flights to the moon between July 1969 and June 1972 brought back a unique assemblage of materials, carrying in them the history of SCR through a variety of radioactive and stable nuclides [2]. What is particularly relevant for retrieving information from these materials, is the care with which the sampling process was recorded by the astronauts during their various missions on the lunar surface.

A schematic presentation of cosmic-ray irradiation on the moon is shown in fig. 1. Both GCR and SCR consist mainly of protons, with the alpha component in SCR [3] substantially lower than the one of GCR [4]. This makes it particularly difficult to observe SCR alpha particles. In general, radionuclides produced by alpha particles are masked by the more abundant production of the same radionuclide through proton-induced reactions. A notable exception is the $^{56}Fe(\alpha,n)^{59}Ni$ reaction in lunar surface material which contains substantially more Fe than Co and Ni. From SCR alpha fluxes measured in solar flares, and the known $^{56}Fe(\alpha,n)^{59}Ni$ cross section, Lanzerotti et al. [6] calculated the production rate of ^{59}Ni on the moon, and compared it with results of ^{59}Ni activity measurements available at the time. Agreement within a factor 4 was obtained.

When AMS evolved as a highly sensitive technique for the detection of long-lived radionuclides, it was

Correspondence to: Dr. W. Kutschera, Physics Division, Argonne National Laboratory, Argonne, IL 60439, USA.

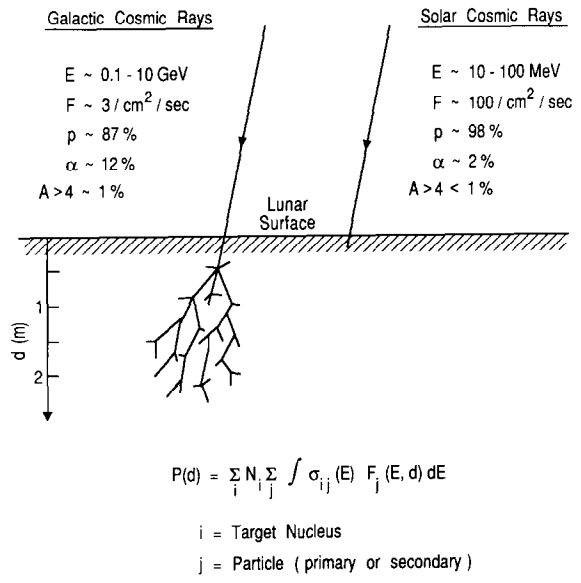

Fig. 1. Schematic presentation of the irradiation of lunar surface with solar cosmic rays (SCR) and galactic cosmic rays (GCR). The high energy of GCR particles generates a secondary particle cascade, since the nuclear interaction length is shorter than the electronic stopping length. The opposite occurs for the SCR particles. Therefore, only nuclear reactions with primary particles have to be considered for SCR. The production rate for a specific radionuclide as a function of depth, $P(d)$, depends on the composition of the bombarded material, N_i, the cosmic-ray flux as a function of energy and depth, $F_j(E, d)$, and on the cross section for reactions between cosmic-ray particles and target nuclei, $\sigma(ij)$. For calculations of production rates see ref. [5].

pointed out on several occasions, e.g. ref. [2], that a more detailed ^{59}Ni measurement should be performed. However, isobaric interference from ^{59}Co makes a ^{59}Ni detection with AMS rather difficult. Earlier attempts to separate ^{59}Ni by full stripping did not reach high sensitivity [7,8] because of low beam energies. In a different approach, interference from ^{59}Co background was substantially reduced through selective ionization of $^{59}Co^-$ ions with photons from a pulsed Nd:YAG laser [9]. Although good separation was achieved, the low duty factor of the pulsed laser has so far prevented ^{59}Ni measurements at natural levels. However, beam energies available now at the Argonne tandem linac accelerator system (ATLAS) make it possible to detect with the full-stripping technique cosmogenic ^{59}Ni in meteoritic and lunar materials. A general description of AMS measurements with ATLAS are given in ref. [10].

In section 2, conditions for AMS with fully stripped ions are reviewed. In section 3, the sample preparation is described. The AMS measurements are presented in section 4. In section 5, the results are discussed, with some outlook for future improvements of the AMS technique, and conclusions are presented in section 6.

2. AMS with fully stripped ions

Shortly after AMS was introduced as a sensitive method for radionuclide detection, Raisbeck et al. [11] applied the full-stripping technique to separate ^{26}Al from the stable isobar ^{26}Mg. It was realized [11] that at sufficiently high energies a separation from isobaric interference can be obtained for those cases where the radionuclide has a higher atomic number than the stable isobar (e.g. $^{26}Al^{13+} - {}^{26}Mg^{12+}$, $^{36}Cl^{17+} - {}^{36}S^{16+}$, $^{41}Ca^{20+} - {}^{41}K^{19+}$, $^{53}Mn^{25+} - {}^{53}Cr^{24+}$, $^{59}Ni^{28+} - {}^{59}Co^{27+}$). Subsequently, this technique was demonstrated for ^{41}Ca [12–15], ^{59}Ni [7,8], ^{26}Al [8,16], ^{36}Cl [8,16], and ^{53}Mn [14]. Except for ^{36}Cl, however, the sensitivity was too low to observe these radionuclides at natural concentrations. This was mainly due to the low overall detection efficiency for the fully stripped ions, primarily caused by low beam energies.

A simple estimate for the energy required for efficient (~ 50%) stripping to the bare nucleus can be obtained from the Bohr criterion [17]. In this approximation, ions have equal probability for losing and capturing an electron in a particular orbit when the ion velocity matches the orbital electron velocity. Applied to hydrogen-like ions, one has the relation $V_{ion} = V_{electron} = Zc/137$. This results in a value for the ion energy of $E = 0.0248AZ^2$ MeV, with A being the mass number and Z the proton number. For ^{59}Ni one thus obtains an energy of 1148 MeV. Actual ion energies required for a 50% full stripping probability are somewhat lower (see below). At ATLAS, the charge-state distribution for Ni and Co beams was measured in the energy range between 600 and 700 MeV. These measurements were performed with the split-pole magnetic spectrograph at 0° with respect to the beam direction. In general, six charge states could be simultaneously observed in the focal plane detector (see fig. 2), which allowed for a quick and reliable charge state distribution measurement. Table 1 summarizes the results of these measurements. The table shows that a foil thickness of about 1–1.5 mg/cm^2 is required to reach the highest abundance for fully-stripped ions. It is assumed that at this thickness charge-state equilibrium has been reached. The most striking result listed in table 1 is the extremely small full-stripping fraction of the Ni beam observed for nickel foils. Systematic measurements with stripper materials around nickel would be necessary to understand this unusual behavior.

For the AMS measurements of ^{59}Ni, carbon foils of 1.30 mg/cm^2 thickness and an energy of 641 MeV

Table 1
Results of charge state distribution measurement

Incident beam			Stripper foil		Charge state fraction [a] [%]					
Isotope	E [MeV]	q	Material	D [mg/cm^2]	28+	27+	26+	25+	24+	23+
^{58}Ni	597	21+	carbon	0.50	5.6	29.6	45.7	16.7	2.3	0.11
				0.93	7.2	34.1	41.7	14.7	2.1	0.15
				1.30	6.4	32.9	42.3	15.6	2.7	0.12
				1.93	5.6	29.4	43.3	18.0	3.3	0.31
			nickel	1.35	0.092	3.6	20.2	40.0	26.9	9.3
				1.81	0.087	2.9	23.7	38.3	26.3	8.8
^{62}Ni	674	20+	carbon	1.30	9.5	38.5	39.5	11.0	1.4	0.14
^{59}Co	641	19+	carbon	1.30		13.4	42.3	34.6	8.6	0.96
^{58}Ni	650	21+	carbon	0.93	10.2	38.0	39.7	10.7	1.4	0.05
				1.30	10.5	39.0	38.4	10.8	1.2	–
				1.93	9.3	38.0	37.6	13.1	1.9	0.1
^{58}Ni	705	21+	carbon	0.10	3.7	23.7	48.4	19.6	3.9	0.7
				0.30	5.6	30.7	46.4	13.9	2.6	0.8
				0.50	10.4	38.6	40.2	10.0	0.8	–
				0.93	13.6	43.0	35.3	7.5	0.68	0.04
				1.30	15.0	44.5	33.0	6.8	0.69	0.03
				1.93	14.1	44.1	33.2	7.7	0.81	0.04
			gold	0.10	0.25	3.07	19.6	31.2	30.5	15.3

[a] Statistical uncertainties for most of the charge state fractions are less than 5% of the respective values, except for fractions below 1% where they are up to a factor of 3 larger.

were chosen. The charge state distribution for ^{59}Ni ions of 641 MeV was measured with ^{62}Ni ions of equal velocity, which corresponds to a ^{62}Ni energy of 674 MeV (fig. 2). The charge state distribution for ^{59}Ni ions cannot be measured directly, because the background of ^{59}Co always obscures charge states $\leq 27^+$ (cf. section 4.3 and fig. 4). However, the measurement with ^{62}Ni is equivalent to a direct measurement with ^{59}Ni, since the charge state distribution for ions of a given atomic number depends on the velocity only, and not on the mass.

In table 2 the full-stripping fraction for carbon foils for which the maximum yield was observed are compared with predictions using the semi-empirical formula of Baudinet-Robinet [18], which is applicable for carbon foils. For this calculation the exit energies from the foils (see table 2) were used. The predicted values are about 50% higher than the measured ones. The latter rise with an energy dependence approximately proportional to E^4, somewhat steeper than the predicted values. Assuming that this trend persists, one estimates for the 50% full-stripping probability an energy of about 950 MeV for ^{58}Ni. The Baudinet-Robinet prediction requires 1010 MeV, and the Bohr estimate 1148 MeV. This comparison shows that currently only experimental data gives reliable information on the fully-stripped fraction of Ni ions as a function of energy.

3. Sample preparation

The main goal of the present ^{59}Ni measurements was to find out whether the full-stripping technique

Table 2
Equilibrium charge-state fraction for full stripping in carbon foils

Ion	Incident energy [MeV]	Carbon foil thickness [mg/cm^2]	Exit energy [MeV]	Q = Z	Full-stripping fraction [%]	
					Measured	Predicted [18]
^{58}Ni	597	0.93	576	28+	7.2	11.8
^{62}Ni	674	1.30	646	28+	9.5	14.7
^{59}Co	641	1.30	615	27+	13.4	18.2
^{58}Ni	650	1.30	622	28+	10.5	16.5
^{58}Ni	705	1.30	678	28+	15.0	22.5

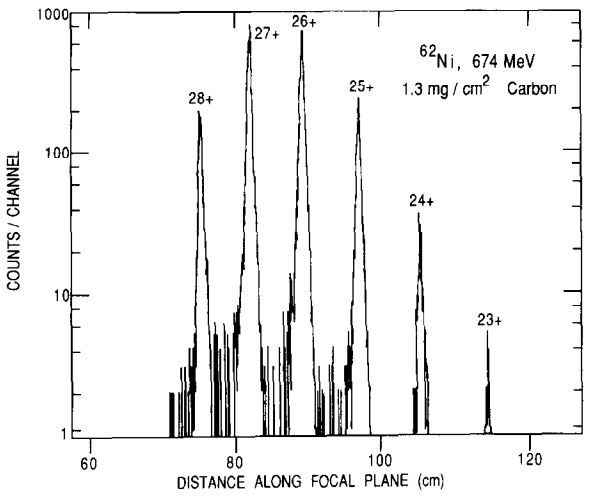

Fig. 2. Charge state spectrum of 674 MeV ^{62}Ni ions after stripping in a 1.3 mg/cm^2 thick carbon foil. The full charge state distribution can be measured simultaneously in the focal plane detector of the split-pole magnetic spectrograph (see table 1 for intensities). The spectrograph was positioned at 0° with respect to the incident ^{62}Ni ions. This charge state distribution is representative for ^{59}Ni at 641 MeV, where ^{59}Ni has the same velocity as ^{62}Ni at 674 MeV.

would allow one to reach the sensitivity to detect ^{59}Ni produced from SCR alpha particles in lunar surface rocks. As an additional test of the method, a meteoritic sample was prepared which was expected to have a higher ^{59}Ni concentration from thermal neutron capture reactions. Important for a reliable measurement was a calibration sample with a known ^{59}Ni/Ni ratio. In addition, blank samples were prepared to check for possible background contributions to the parameter space where ^{59}Ni events were observed.

3.1. Lunar rock 68815

Apollo 16 lunar rock 68815 is a breccia that was collected from near the top of a boulder of 1 m height [19,20]. The ^{81}Kr–Kr exposure age for this rock is 2.0 million years [21] indicating that it was probably ejected by the South Ray crater event. Depth profile studies of cosmogenic nuclides have been performed on sample 234 of rock 68815. ^{26}Al and ^{53}Mn were measured by Kohl et al. [22] followed by a study of ^{10}Be profiles by Nishiizumi et al. [23]. Sample 234 was divided into three subsamples (A, B, and C), which had different zenith angles (A: 48 ± 16°, B: 41 ± 17°, and C: 29 ± 15°). Each subsample was ground to four different nominal depths (0–0.5, 0.5–1.0, 1.0–2.0, and 2.0–4.0 mm). The details of the grinding procedure are described by Kohl et al. [22]. In the present work we chose surface sample 68815-1A (0.847 g) which came from a depth of 0–0.5 mm (0.14 g/cm^2) on face A. 68815-1A contains 4.28% Fe and 1100 ppm Ni. Cobalt concentration in 68815 is 30 ppm [24]. The nickel was separated from an aliquot sample that was previously dissolved for ^{26}Al and ^{53}Mn measurements [22]. The nickel fraction was recovered from an elutant of a cation exchange column that was used for Be and Al separation [22]. The solution was evaporated to dryness and boiled with aqua regia to decompose organic materials. Then the sample was dissolved with dilute HCl. The solution was treated with 20 ml of 50% ammonium citrate which acts as a masking reagent, and with NH_4OH to make a solution of pH ~ 7. The sample solution was transferred to a separatory funnel and 25 ml of 0.1% dimethylglyoxime solution was added. The Ni dimethylglyoxime complex was back extracted into 25 ml of 2 N HCl. In order to obtain a sufficiently large Ni sample for the AMS measurement, 21 mg of Ni carrier were added at this point, resulting in a total Ni amount of 22 mg. The Ni was further separated from Co using an anion exchange column eluted with 9 N HCl. Then Ni was converted to nitrate in a small quartz crucible and ignited to NiO at 1000°C. The oxide was cooled to room temperature under a dry nitrogen flow. NiO was reduced to Ni metal since the metal gives a higher Ni^- current than does NiO in the Cs-beam sputter source (see section 4.1). The reduction was performed by heating NiO in a quartz crucible for 1 h to 600°C in a hydrogen flow, resulting in 19.4 mg Ni metal available for the AMS measurement. In the same way, a chemical blank (34.7 mg) was prepared from the reagent Ni used as carrier material.

3.2. Admire meteorite

Admire is a stony-iron meteorite (pallasite) which was found in Kansas in 1881. The recovered mass is over 80 kg. The exposure age of the meteorite is calculated to be 130 million years [25]. The nickel used for this study was an aliquot of the sample used by Honda et al. [25], who measured a ^{59}Ni activity of 300 ± 30 dpm ^{59}Ni/kg metal by low-level X-ray counting. The Ni for the present work was stripped off the plated X-ray counting sample. All chemical procedures were the same as those used for 68815, excluding the Ni dimethylglyoxime extraction. According to Buseck [26], Admire contains 51.5% Fe (metal) and 6.9% Ni. With a ^{59}Ni half-life of $(7.6 \pm 0.5) \times 10^4$ yr [27], 300 ± 30 dpm ^{59}Ni/kg metal can be converted to 2.54 ± 0.25 dpm/g Ni or $(1.43 \pm 0.17) \times 10^{-11}$ ^{59}Ni/Ni.

3.3. Neutron-irradiated nickel metal

A sample was prepared from high purity nickel powder [28] enriched in ^{59}Ni by neutron activation [29]. From the neutron flux measured with a Au monitor

foil and the cross section for the ^{58}Ni(n,γ)^{59}Ni reaction, a ^{59}Ni/Ni ratio of 3.08×10^{-11} was calculated. In a recent AMS experiment [30] at the 14UD Pelletron tandem at ANU (Canberra), an absolute ^{59}Ni/Ni ratio of $(2.45 \pm 0.33) \times 10^{-11}$ was measured for this material. In addition to this calibration material, we also prepared a blank from the same, nonirradiated Ni powder.

4. AMS measurements

The AMS measurements were performed with the ATLAS accelerator system [10]. Negative ions from the sputter source are mass-analyzed in a 90° double focussing magnet, preaccelerated to 150 keV, accelerated in an FN tandem accelerator, subsequently boosted to higher energy in a linear accelerator based on superconducting resonators, and finally detected with a split-pole magnetic spectrograph.

Since both the lunar and meteoritic samples were available as NiO, we first determined the performance of our SNICS II Cs-beam sputter source [31] for the production of Ni^- beams from NiO and Ni metal.

4.1. Production of Ni^- beams from Ni metal and NiO

Sample holders for the sputter source were prepared from copper with a geometry shown in fig. 3. It is similar to the one described in Middleton's "negative ion cookbook" [32]. Our SNICS II source is equipped with a spherical ionizer which produces a small beamspot of less than 1 mm diameter. 20 to 30 mg of Ni or NiO powder were firmly pressed into the 1.6 mm diameter sample hole, leaving a depression of approximately 0.5 mm. This helped to reach the maximum Ni^- current in a relatively short time (~ 10 min) for a newly prepared sputter sample. From Ni metal powder samples, $^{58}Ni^-$ currents of 5 μA were measured at the entrance of the tandem accelerator. Samples prepared from pure NiO and NiO mixed with Ag powder both resulted in $^{58}Ni^-$ currents of about 1 μA. In addition to the lower Ni^- output, the emittance also seemed to be larger, perhaps caused by space charge effects of a strong $^{16}O^-$ beam emerging from the NiO material. We therefore decided to use only Ni in metal form for the ^{59}Ni/Ni ratio measurements. It is known that Ni has a rather high sputter yield, which means that the sample material is consumed quickly. Under AMS running conditions, we chose a compromise between Ni^- output and lifetime of the material by reducing the Cs sputter beam intensity. With these conditions, the sputter rate was approximately 4 mg/h, which required a relatively large dilution of the lunar sample with Ni carrier (section 3.1.). In view of the low Ni content in lunar rock, a reduction of the consumption rate to values of 0.5 to 1 mg/h, more typical for AMS of other long-lived radionuclides, would be desirable.

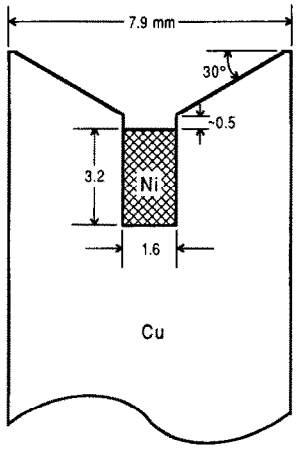

Fig. 3. Geometry of the sample holder for the SNICS II Cs-beam sputter source. All dimensions are in millimeters. Individual amounts of sample material used in these holders varied between 20 and 30 mg.

4.2. Experimental procedure

The ATLAS accelerator was tuned for ^{59}Ni with a pilot beam of ^{62}Ni. Choosing a charge state combination of 1^- (ion source) $\rightarrow 11^+$ (tandem terminal) $\rightarrow$ 20^+ (linac injection) for ^{62}Ni, and $1^- \rightarrow 10^+ \rightarrow 19^+$ for ^{59}Ni, it is possible to obtain the same velocity for both isotopes at the linac entrance with only a minor tandem voltage adjustment. Since the mass/charge ratio of $^{59}Ni^{19+}$ and $^{62}Ni^{20+}$ ions differ only by 1.74×10^{-3}, the two beams were expected to be equivalent in all aspects of linac acceleration and beam transport. However, it turned out that the ^{62}Ni tune did not simulate ^{59}Ni acceleration sufficiently close. We therefore decided to use the stable isobar ^{59}Co, produced from a source material containing 10% cobalt and 90% nickel. The mass/charge ratio of $^{59}Co^{19+}$ differs by only 1.95×10^{-5} from $^{59}Ni^{19+}$, which allows one to tune the entire system very well for ^{59}Ni detection. This procedure, however, increased the ^{59}Co background through memory effects in the source by several orders of magnitude. Fortunately, the full-stripping technique produced a physical separation of $^{59}Ni^{28+}$ ions from the ^{59}Co background in the focal plane of the split-pole spectrograph. This allows one to block the majority of ^{59}Co ions from entering the sensitive focal plane detector. Absolute values of ^{59}Ni/Ni ratios could not be measured in the experiment because of apparent losses resulting from the vertical detector acceptance.

^{59}Ni/Ni ratios of the unknown samples were measured relative to the calibration sample (section 3.3.) by

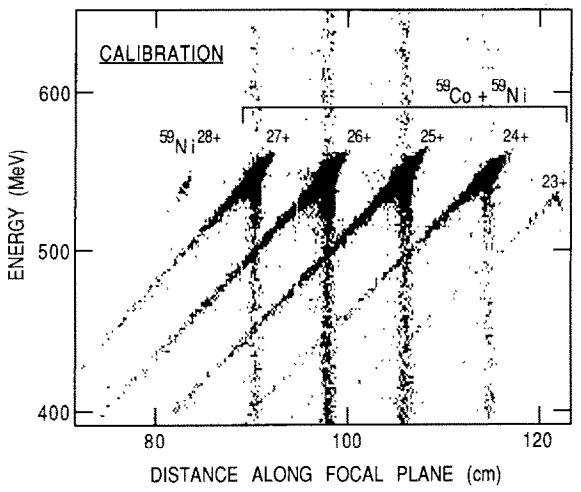

Fig. 4. Two-dimensional display of energy vs focal plane position for events measured from the ^{59}Ni calibration sample with a ^{59}Ni/Ni ratio of 2.5×10^{-11}. The energy, measured with the Bragg-curve detector, is reduced with respect to the beam energy by energy losses in the stripper foil and the parallel plate avalanche detector. Details about the structure of the spectrum are discussed in section 4.3. The spectrum was measured before a ^{59}Co beam was used for tuning of the accelerator system. The ^{59}Co/^{59}Ni ratio is approximately 800.

measuring for each sample the $^{58}Ni^-$ current at the tandem entrance before and after a ^{59}Ni counting period in the split-pole spectrograph. Individual counting periods lasted 0.5–1 h, with total counting times per sample of up to 2 h. To ensure a reliable measurement of the $^{59}Ni^{28+}$ counting rate, an "out-of-lock" master trigger disabled data taking including a timing scaler when the tandem terminal voltage deviated by more than ± 10 kV from its nominal value of 8.630 MV, or when the phase or amplitude of a linac resonator went outside the range required for proper acceleration of ^{59}Ni ions.

4.3. Results of the ^{59}Ni / Ni measurements

Spectra of ^{59}Ni and ^{59}Co ions were measured with a focal plane detector system [33] consisting of a low-pressure position-sensitive parallel plate avalanche counter (5 Torr isobutane, C_4H_{10}) and a Bragg-curve ionization chamber (196 Torr freon, CF_4) for Z identification and energy measurement. Fig. 2 shows the charge-state distribution of ^{62}Ni ions. This measurement was performed with a ^{62}Ni beam of the same velocity as the ^{59}Ni ions (see table 2). After ATLAS was tuned with ^{62}Ni for ^{59}Ni acceleration, the ^{59}Co background was low enough to accept ions over the full focal plane range. Fig. 4 shows a two-dimensional spectrum of energy versus focal-plane position from the calibration sample measured with this condition. As can be seen, the $^{59}Ni^{28+}$ peak is clearly separated from the ^{59}Co background, in spite of unavoidable tailing typical for the heavy ion detection with magnetic spectrographs at 0° scattering angle [34]. The diagonal tails are due to ions which enter the spectrograph with lower energies mainly from slit scattering. The vertical tails are due to pileup effects and to electron–ion recombination in the Bragg curve detector.

As discussed in section 4.2, a ^{59}Co isobaric beam had to be used for a reliable setup of ATLAS for ^{59}Ni detection. This increased the ^{59}Co background to an extent that the majority of ^{59}Co ions had to be blocked from entering the focal plane detector. Shortly after the ^{59}Co tuning, the ^{59}Co background intensity from a nickel sample was approximately 1.5×10^5 ^{59}Co ions/s at the carbon stripper foil position at the entrance of the spectrograph. This corresponds to a $^{59}Co^-/^{58}Ni^-$ ratio of about 3×10^{-6} from the ion source. Compared to the conditions before the use of a ^{59}Co beam (cf. fig. 4), this is an increase of the ^{59}Co background by 3 orders of magnitude.

The first series of ^{59}Ni/Ni measurements were performed 7 h after the ^{59}Co tuning when the ^{59}Co background had decreased by about a factor of 30. The results are shown in figs. 5a–5c. No background events are seen within the ^{59}Ni peak region for a blank sample (fig. 5b). Fig. 6 displays the spectrum of fig. 5c, Admire meteorite, in a three-dimensional way, which more explicitly shows the very clean separation of $^{59}Ni^{28+}$ ions from the ^{59}Co background. Spectra of figs. 5d–5f display a much higher ^{59}Co background. This was due to a much shorter waiting period between a new ^{59}Co tune and the ^{59}Ni/Ni ratio measurements. With the higher ^{59}Co background, there is a clear indication of ^{59}Ni events originating from charge exchange reactions of ^{59}Co with the carbon stripper foil. Fortunately, because of the large negative Q value of -14.4 MeV for the $^{12}C(^{59}Co, ^{59}Ni)^{12}B$ reaction, these events do not interfere with the ^{59}Ni peak from the source sample. This is evident from fig. 5e, where no background events are present for a blank sample in the relevant ^{59}Ni region. An order-of-magnitude estimate for the center-of-mass cross section of the $^{12}C(^{59}Co, ^{59}Ni)^{12}B$ reaction from these spectra gave a value of about 10 mb/sr. This assumed a (poorly measured) ^{59}Co intensity of several hundred thousand ions per second incident on the 1.3 mg/cm^2 thick carbon stripper, a laboratory solid angle of 5.4×10^{-3} sr, and a $^{59}Ni^{28+}$ charge state fraction of 10%. In addition to the charge exchange reaction, various neutron and/or proton transfer reactions may take place between ^{59}Co and ^{12}C. Indications of events originating from such reactions can be seen in figs. 5d–5f as mass lines between those from mass 59 ($q = 28^+$, 27^+, 26^+). Fig. 5f shows the result for the lunar rock sam-

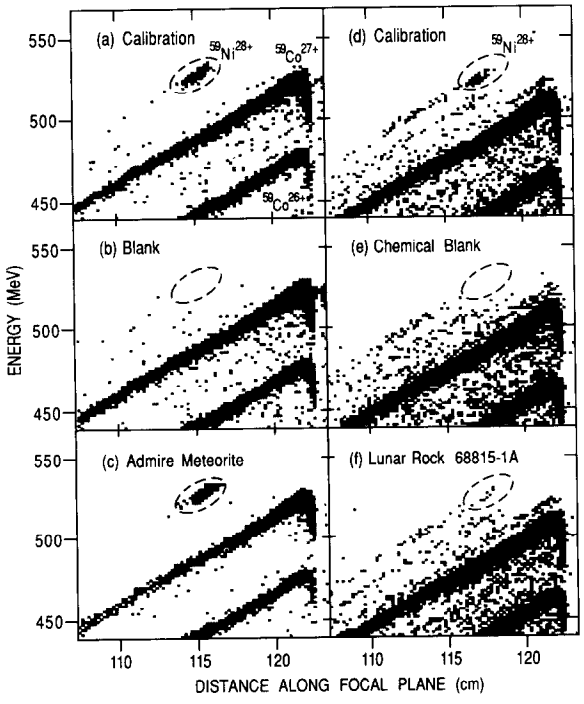

Fig. 5. Summary of two-dimensional spectra of energy vs focal plane position measured for various samples. Identical software windows were applied to all spectra to count the $^{59}Ni^{28+}$ events, as indicated by the dashed lines. Due to a high ^{59}Co background from ^{59}Co-beam tuning, the ions were shifted in their focal plane position by lowering the magnetic field strength, in order to cut off most of the ^{59}Co background ions (compare with fig. 4). A particularly high ^{59}Co intensity appears in spectra (d)–(f) which were taken shortly after retuning the system with ^{59}Co. In order to reduce the ^{59}Co counting rates to an acceptable level in the focal plane detector, the magnetic field strength was further lowered cutting off more of the ^{59}Co ions. The low-energy tail of $^{59}Ni^{28+}$ ions is due to the charge exchange reaction $^{12}C(^{59}Co, ^{59}Ni)^{12}B$ (see text for details).

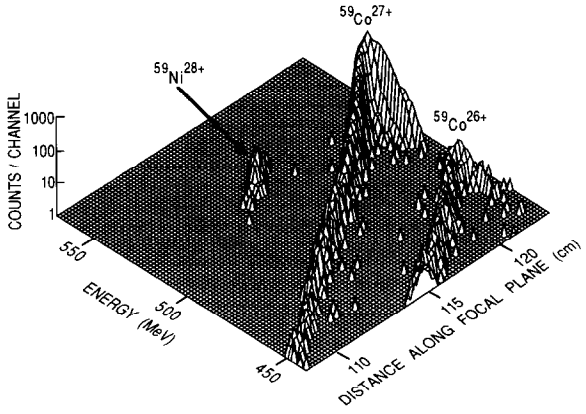

Fig. 6. Three-dimensional presentation of the spectrum measured from the Admire meteorite, shown also in fig. 5c. The very clean separation of ^{59}Ni from ^{59}Co background is apparent.

ple. Although the background is large, we can clearly identify genuine ^{59}Ni events from the sample.

The results of the ^{59}Ni/Ni ratio measurements are summarized in table 3. The results are in the order they were measured and displayed in figs. 5a through 5f. The somewhat lower $^{58}Ni^-$ intensity as compared to the source tests described in section 4.1 is due to (i) a lower Cs-sputter current (in order to stretch the lifetime of the precious lunar sample material), (ii) a lower yield from reduced NiO samples as compared to commercial Ni metal powder, and (iii) a gradual drop of Ni^- output during the running time of several hours.

5. Discussion

The results presented in section 4 demonstrate that ^{59}Ni/Ni ratios in the range of 10^{-13} to 10^{-11} can be

Table 3
Results of ^{59}Ni/Ni ratio measurements

Sample	$^{58}Ni^-$ [μA]	Counting time [min]	$^{59}Ni^{28+}$ [counts]	Counting rate [$^{59}Ni^{28+}$/(min μA $^{58}Ni^-$)]	^{59}Ni/Ni [10^{-13}]
Neutron-irradiated nickel (calibration)	3.6	64.3	146	0.63	245 ±33 [a]
Nonirradiated nickel (blank)	4.3	123.8	0	< 0.0019	< 0.73 [b]
Admire meteorite	3.9	63.9	149	0.60	230 ±40 [c]
Neutron-irradiated nickel (calibration)	2.0	38.1	56	0.73	245 ±33 [a]
Chemical blank	3.2	124.7	0	< 0.0025	< 0.84 [b]
Lunar rock 68815-1A	2.8	121.4	9	0.026	8.8± 3.3 [c]

[a] Calibration sample. The quoted ^{59}Ni/Ni ratio is from Paul et al. [30].
[b] Upper limit calculated assuming one $^{59}Ni^{28+}$ count.
[c] Uncertainties are calculated by adding in quadrature the given uncertainty from the calibration value (last column) and from statistical uncertainties of the observed $^{59}Ni^{28+}$ events (column 4) for both the calibration and the unknown sample.

measured by full-stripping AMS in the present setup. This sensitivity is adequate for meteoritic samples but not for lunar samples with lower ^{59}Ni content than measured here. Much lower ^{59}Ni concentrations are expected for layers beyond 0.14 g/cm^2 ($\sim$0.5 mm) depths [6,38]. In the following, we first discuss the relevance of the present results with respect to their information on meteoritic and SCR-related aspects (lunar sample). We then present possibilities to improve on the current AMS technique, with the goal to reach a sensitivity which would allow one to measure a detailed profile of ^{59}Ni produced by SCR alpha particles in lunar rock.

5.1. ^{59}Ni production in meteorites

Meteorites and lunar samples are the prime storehouses for the cosmic-ray record in the past [1]. The information is stored in a time-integrated way through the production of radionuclides of different half-lives by nuclear reactions of cosmic ray primary and secondary particles with nuclei of the meteorite or the lunar sample. Depending on the half-life, the production mechanism, and the composition and size of the meteorite, radionuclides probe properties of cosmic rays and/or of the meteorite itself. Most ^{59}Ni is produced in meteorites by the reaction ^{58}Ni(n,γ)^{59}Ni. The thermal neutron capture cross section for ^{58}Ni (68.3% abundance) is 4.6 b. Therefore, ^{59}Ni would be very useful in determining the preatmospheric size of a meteorite and the depth of a specific sample since the thermal neutron flux produced by GCR interactions in the meteorite depends on these size parameters [35,36]. A combination of such a measurement with results of other thermal neutron products such as ^{36}Cl, ^{41}Ca, and ^{60}Co would be particularly valuable.

The observed ^{59}Ni/Ni ratio in the Admire meteorite, $(2.3 \pm 0.4) \times 10^{-11}$, can be converted to 4.1 ± 0.7 dpm ^{59}Ni/g Ni or 490 ± 80 dpm ^{59}Ni/kg metal. Our measured value is about 50% higher than that of Honda et al. [25] for the same sample (see section 3.2). Honda et al. [25] found that the concentrations of spallogenic radionuclides in Admire are about one half of those in the small iron meteorite Aroos (Yardymly) due to the heavier shielding in Admire. One might expect higher thermal neutron fluxes in Admire but the observed ^{59}Ni concentration, 4.1 dpm/g Ni, implies a lower neutron flux than the one derived from theoretical calculations [35,36]. Although the low ^{59}Ni can be explained by a long terrestrial age, measurements of other nuclides produced by thermal neutron capture such as ^{36}Cl in the stony phase of this meteorite must be obtained to make further discussion meaningful. ^{59}Ni/Ni values in the 10^{-11} range have recently been measured in meteoritic samples by other AMS techniques [30,37].

5.2. The ^{56}Fe(α,n)^{59}Ni reaction in lunar material

Using the known amount of Ni carrier added to the lunar sample 68815-1A and the Ni concentration of the sample, we obtain $(2.4 \pm 0.9) \times 10^{11}$ atoms ^{59}Ni/kg rock or 4.1 ± 1.5 dpm ^{59}Ni/kg rock from our measured ^{59}Ni/Ni ratio shown in table 3. The majority of the ^{59}Ni in the surface of the moon must be ascribed to production by SCR alpha particles on Fe, probably $> 95\%$ due to the ^{56}Fe(α,n)^{59}Ni reaction. The contribution from ^{59}Co(p,n)^{59}Ni and ^{60}Ni(p,pn)^{59}Ni reactions by SCR protons, and ^{58}Ni(n,γ) and ^{60}Ni(n,2n) reactions by GCR secondary particles are negligible for the surface sample 68815-1A because of the low concentration of the target elements Co and Ni in lunar samples. The specific activity in this sample is 95 ± 36 dpm ^{59}Ni/kg Fe based on an Fe concentration of 4.28% in sample 68815-1A. Since the exposure age of the rock, 2.0 million years [21], is long enough to saturate ^{59}Ni production, the measured ^{59}Ni concentration is equivalent to an average ^{59}Ni production rate of 95 ± 36 atoms/(min kg Fe). Although the uncertainty is large due to poor statistics, this value compares well with the ^{59}Ni production rate calculated by Reedy [38] for the ^{56}Fe(α,n)^{59}Ni reaction induced by SCR alpha particles. In this calculation, an omnidirectional flux normalization of 10 α/(cm^2 s) for energies above 10 MeV was assumed. The flux, J, was assumed to have an exponential dependence on the rigidity, R, $\mathrm{d}J/\mathrm{d}R = \text{const}\ \exp(-R/R_0)$. The resulting ^{59}Ni production rate drops sharply from 1220 atoms/(min kg Fe) at the surface to 18 at a depth of 0.20 g/cm^2. These values are based on a spectral shape parameter of $R_0 = 75$. With a slightly stiffer flux dependence, $R_0 = 100$, the corresponding values are 1016 and 27 atoms/(min kg Fe). The average ^{59}Ni production rate from Reedy's [38] calculation for our sample thickness is about 180 without erosion, as compared to the measured value of 95 ± 36. The equilibrium activity of ^{59}Ni is reduced to about 25 atoms/(min kg Fe) for our sample depth assuming an erosion rate of 1 mm/Myr. The erosion rate in rock 68815 has been determined from the ^{26}Al and ^{53}Mn depth profiles to be 1.3 to 3 mm/Myr [22,23]. The observed ^{59}Ni result may result from a lower erosion rate or a higher solar alpha flux for the last 100 000 years. Clearly, more measurements are required for such a detailed discussion. Only one ^{59}Ni measurement in lunar bulk fines, sample 10084,16, has been previously reported [39]. It is interesting to note that the observed value of 3.3 ± 1.0 dpm ^{59}Ni/kg sample or 27 ± 8 dpm ^{59}Ni/kg Fe is relatively high considering the sample depth of these fines, which extends from the surface to more than a few centimeters. Future measurements of ^{59}Ni in lunar surface soils may contribute to the study of relatively short term lunar surface "gardening".

It has also been suggested [40] that cosmic dust might be a useful target material for the ^{56}Fe(α,n)^{59}Ni reaction. In deep-sea sediments, a specific ^{59}Ni activity of $(5.9 \pm 1.8) \times 10^{-2}$ dpm/kg sediment was found [41], and ascribed to the production of ^{59}Ni by SCR protons (~ 20%) and alpha particles (~ 80%). With a substantial improvement of the AMS technique, it may eventually become feasible to study small samples of cosmic dust and individual cosmic spherules directly for their ^{59}Ni content.

5.3. Improvements for AMS measurements of ^{59}Ni

Our ^{59}Ni/Ni ratio measurements demonstrated that the full-stripping technique is capable of reaching sensitivities of 10^{-13} for ^{59}Ni detection essentially background-free. From the known ^{59}Ni/Ni ratio of the calibration sample and the measured parameters presented in table 3, one calculates an overall detection efficiency of $^{59}Ni^{28+}/^{59}Ni^{-} = 0.7 \times 10^{-4}$. This low value is largely due to the fact that three stripping processes were involved: $1^- \rightarrow 10^+$ (tandem terminal), $10^+ \rightarrow 19^+$ (between tandem and linac), and $19^+ \rightarrow 28^+$ (split-pole spectrograph). In addition, intensity losses occur in the linac acceleration because the pre-tandem buncher cannot be used. The buncher requires a phase feedback signal from a measurable beam after tandem acceleration. Further intensity losses occur in the present focal plane detector since the vertical image of the ^{59}Ni beam, widened by angular straggling in the thick carbon stripper foil, is larger than the detector entrance window.

A number of possible improvements should allow one to increase the detection limit by at least 1 order of magnitude, and perhaps eventually by 2: (i) a focal plane detector with a larger vertical window may yield a factor of 2–3; (ii) higher beam energy of about 800 MeV should result in an increase of full-stripping probability also by about a factor of 3; (iii) the use of the ECR source with the new ATLAS positive ion injector replacing tandem injection [10] could provide improvements in several ways: the full bunching capability can be used, which may gain as much as a factor of 5 in intensity compared to tandem injection without pre-tandem bunching. In the ECR source, Ni from small samples may be converted into high charge state ions in a more efficient way than is currently possible with the combination of a Cs-beam sputter source and stripping in the tandem terminal. All of this may well lead to ^{59}Ni/Ni ratio measurements in the 10^{-15} range, desired for performing a detailed ^{59}Ni depth profile measurement in lunar material.

In recent AMS measurements of ^{59}Ni at other laboratories [30,37], it has been demonstrated that ^{59}Ni/Ni ratios in the 10^{-11} range can be well measured with a large tandem alone, without using fully stripped ions. Although the overall efficiency of these systems is substantially larger, it has to be seen whether the omnipresent background of ^{59}Co can be reduced to such a low level that ratio measurements several orders of magnitude lower than 10^{-11} are possible.

6. Conclusion

Using an AMS full-stripping technique at high energy, ^{59}Ni produced by solar cosmic ray alpha particle interacting with the surface of lunar rock have been observed. This result encourages us to improve the AMS technique to the extent where a depth profile of ^{59}Ni in lunar rock could be measured. Such a measurement would provide a unique window to the history of energetic helium emission from the sun.

Acknowledgement

We thank M. Honda and C.P. Kohl for initial chemical separation of Admire and 68815 samples, E. Kanter for charge state calculations, G. Korschinek for providing information on ^{59}Ni measurements prior to publication, and W. Henning for valuable discussions. This work was supported by the US Department of Energy, Nuclear Physics Division, under contract W-31-109-Eng-38, and NASA grant NAG9-33.

References

[1] R.C. Reedy, J.R. Arnold and D. Lal, Science 219 (1983) 127.
[2] R.C. Reedy and K. Marti, in: The Sun in Time, eds. C. Sonett and M.S. Matthews (University of Arizona Press, 1991).
[3] R.E. McGuire, T.T. Rosvinge and F.B. McDonald, Astrophys. J. 301 (1986) 938.
[4] J.A. Simpson, Annu. Rev. Nucl. Part. Sci. 33 (1983) 323.
[5] R.C. Reedy and J.R. Arnold, J. Geophys. Res. 77 (1972) 537.
[6] L.J. Lanzerotti, R.C. Reedy and J.R. Arnold, Science 179 (1973) 1232.
[7] W. Henning, W. Kutschera, B. Myslek-Laurikainen, R.C. Pardo, R.K. Smither and J.L. Yntema, Proc. 2nd Int. Symp. on Accelerator Mass Spectrometry, Argonne National Laboratory Report ANL/PHY-81-1 (1981) p. 320
[8] H. Faestermann, K. Kato, G. Korschinek, P. Krauthan, E. Nolte, W. Ruehm and L. Zerle, Nucl. Instr. and Meth. B50 (1990) 275.
[9] D. Berkovits, E. Boaretto, G. Hollos, W. Kutschera, R. Naaman, M. Paul and Z. Vager, Nucl. Instr. and Meth. B52 (1990) 378.
[10] W. Kutschera, I. Ahmad, P.J. Billquist, B.G. Glagola, R.C. Pardo, M. Paul, K.E. Rehm and J.L. Yntema, Nucl. Instr. and Meth. B42 (1989) 101.

[11] G.M. Raisbeck, F. Yiou and C. Stephan, J. Phys. (Paris) 40 (1979) L241.
[12] G.M. Raisbeck and F. Yiou, Rev. Archeometrie 4 (1980) 121.
[13] A. Steinhof, W. Henning, M. Mueller, E. Roeckl, D. Schuell, G. Korschinek, E. Nolte and M. Paul, Nucl. Instr. and Meth. B29 (1987) 59.
[14] G. Korschinek, H. Morinaga, E. Nolte, E. Preisenberger, U. Ratzinger, A. Urban, P. Dragovitsch and S. Vogt, Nucl. Instr. and Meth. B29 (1987) 67
[15] A. Steinhof, W. Henning, M. Mueller, E. Roeckl, D. Schuell, J. Speer, W. Kutschera and M. Paul, Nucl. Instr. and Meth. B52 (1990) 391.
[16] G.W.A. Newton, T.W. Aitken, T.R. Charlesworth, R.A. Cunningham, P.V. Drumm, J.S. Lilley and M.J. Smithson, Nucl Instr. and Meth. B52 (1990) 290.
[17] N. Bohr, Phys. Rev. 58 (1940) 654.
[18] Y. Baudinet-Robinet, Nucl. Instr. and Meth. 190 (1981) 197.
[19] Apollo Field Geology Investigation Team, Science 179 (1973) 62.
[20] Apollo 16 Preliminary Examination Team, Science 179 (1973) 23.
[21] R.J. Drozd, C.M. Hohenberg, C.J. Morgan and C.E. Ralston, Geochim. Cosmochim. Acta 38 (1974) 1625.
[22] C.P. Kohl, M.T. Murrell, G.P. Russ III and J.R. Arnold, Proc. 9th Conf. on Lunar Planet. Sci. (1978) p. 2299.
[23] K. Nishiizumi, M. Imamura, C.P. Kohl, H. Nagai, K. Kobayashi, K. Yoshida, H. Yamashita, R.C. Reedy, M. Honda and J.R. Arnold, Proc. 18th Conf. on Lunar Planet. Sci. (1988) p. 79.
[24] H. Wänke, H. Palme, H. Baddenhausen, G. Dreibus, E. Jagoutz, H. Kruse, B. Spettel, F. Teschke and R. Thacker, Proc. 5th Lunar Conf. (1974) p. 1307.
[25] M. Honda, S. Umemoto and J.R. Arnold, J. Geophys. Res. 66 (1961) 3541.
[26] P.R. Buseck, Geochim. Cosmochim. Acta 41 (1977) 711.
[27] K. Nishiizumi, R. Gensho and M. Honda, Radiochim. Acta 29 (1981) 113.
[28] Johnson–Matthey JMC 891 Specpure, batch number S89676.
[29] We are grateful to Dr. D. Fink for having made this material available to us.
[30] M. Paul, Proc. 6th Int. Conf. on Electrostatic Accelerators and Associated Boosters, Montegrotto, Italy, 1–5 June 1992, Nucl. Instr. and Meth., to be published.
[31] Manufactured by National Electrostatic Corporation, Middleton, WI 53562, USA.
[32] R. Middleton, A Negative Ion Cookbook (University of Pennsylvania, 1989), unpublished.
[33] K.E. Rehm and F.L.H. Wolfs, Nucl. Instr. and Meth. A273 (1988) 262.
[34] T.R. Ophel, L.K. Fifield, W.N. Catford, N.A. Orr, C.L. Woods, A. Harding and G.P. Clarkson, Nucl. Instr. and Meth. A272 (1988) 734.
[35] M.S. Spergel, R.C. Reedy, O.W. Lazerath, P.W. Levy and L.A. Slatest, Geophys. Res. B91 (1986) D483.
[36] P. Eberhardt, J. Geiss and H. Lutz, in: Earth Science and Meteoritics, eds. J. Geiss and E.D. Goldberg (North-Holland, 1963) p. 143.
[37] B. Bante, T. Faestermann, A. Gillitzer, S. Kastel, K. Knie, G. Korschinek and D. Müller, Jahresbericht 1991, Beschleuniger laboratorium der Universität und der Technischen Universität München, p. 90; to be published.
[38] R.C. Reedy, Proc. 21st Conf. on Lunar Planet. Sci. (1990) p. 1003.
[39] J. Shedlovsky, M. Honda, R. Reedy, J. Evans, D. Lal, R. Lindstrom, A. Delany, J. Arnold, H. Loosli, J. Fruchter and R. Finkel, Proc. Apollo 11 Lunar Sci. Conf. (1970) p. 1503.
[40] H. Hasegawa, K. Yamakoshi, M. Noma and T. Maihara, Can. J. Phys. 46 (1968) S930.
[41] K. Yamakoshi and S. Yanagita, Earth Planet. Sci. Lett. 52 (1981) 259.